HHS Public Access

Author manuscript

ACS Nano. Author manuscript; available in PMC 2020 February 26.

Published in final edited form as:

ACS Nano. 2019 February 26; 13(2): 1272–1283. doi:10.1021/acsnano.8b06572.

Neutrophil Membrane-Derived Nanovesicles Alleviate Inflammation to Protect Mouse Brain Injury from Ischemic Stroke

Xinyue Dong[1], **Jin Gao**[1], **Can Yang Zhang**[1], **Christopher Hayworth**[2], **Marcos Frank**[2], and **Zhenjia Wang**[1,*]

[1]Department of Pharmaceutical Sciences, College of Pharmacy and Pharmaceutical Sciences, Washington State University, Spokane, Washington 99202, USA

[2]Department of Biomedical Sciences, Elson S. Floyd College of Medicine, Washington State University, Spokane, Washington 99202, USA

Abstract

Ischemic stroke is an acute and severe neurological disease, resulting in the disability and death. Reperfusion to an ischemic brain is a means to reverse brain damage after stroke; however, this causes secondary tissue damage induced by inflammation responses, called ischemia/reperfusion (I/R) injury. Adhesion of neutrophils to endothelial cells underlies the initiation of inflammation in I/R. Inspired by this interaction, we report a drug delivery system comprised of neutrophil membrane-derived nanovesicles loaded with Resolvin D2 (RvD2) that can enhance resolution of inflammation, thus protecting brain damage during ischemic stroke. In the study, the middle cerebral artery occlusion (MCAO) mouse model was developed to mimic ischemic stroke. Using intravital microscopy of live mouse brain, we real time visualized the binding of nanovesicles to inflamed brain vasculature for delivery of therapeutics to ischemic stroke lesions. We also observed that RvD2-loaded nanovesicles dramatically decreased inflammation in ischemic stroke and improved mouse neurological functions. Our study provides a strategy to inhibit neuroinflammation using neutrophil-derived nanovesicles for ischemic stroke therapy.

Keywords

nanovesicles; resolvin D2; neutrophils; stroke; ischemic/reperfusion injury

Stroke is an acute and severe disease, resulting in the disability and death. It is reported that 80% strokes are related to brain ischemia, which is the blood vessel occlusion leading to a sudden disruption of circulation in a partial brain.[1,2] Reperfusion, a blood flow restoration, is a major tool to treat ischemic stroke to rescue brain functions. However, ischemia/reperfusion (I/R) initiates several cellular responses in the brain. The responses include

*Corresponding Author: zhenjia.wang@wsu.edu.

The authors declare no competing financial interest.

Supporting Information: Supporting Information is available online with supplementary results in stability of nanovesicles, mass spectroscopy and HPLC of RvD2 in nanovesicles, quantification of uptake of nanovesicles by HUVECs, biodistribution studies, cytotoxicity of nanovesicles *in vitro*, analysis of ICAM-1 in brain, a full panel of brain slices, and detailed description of all the movies.

accumulation of aerobic metabolites and production of radical oxygen species, such as O_2^- and H_2O_2. In addition, inflammatory cytokines are upregulated, endothelial cells are activated and immune cells migrate from circulation to the brain tissues.[3–6] These events cause cellular damage in the brain, so-called ischemia/reperfusion (I/R) injury.[7] Interactions between blood vessel endothelial cells and neutrophils (most abundant leukocytes in blood) play a central role in cerebral I/R.[8] For example, upregulation of cell adhesion molecules on endothelium mediates neutrophil transmigration to I/R lesions, leading to irreversible brain damage.[9] To avoid inflammatory damage related to neutrophil infiltration, blocking endothelium *via* anti-ICAM-1 (intercellular adhesion molecule 1), and depleting neutrophils with antibodies were used to mitigate I/R injury in stroke.[10,11] However, inhibiting neutrophil adhesion to blood vessels *via* anti-ICAM-1 is not sufficient to diminish inflammation to prevent I/R injury.[12] In addition, systemic depletion of neutrophils may increase the host susceptibility to infections,[13] and may also impair other immune cells, such as natural killer cells.[14]

Advances in nanoparticle-based drug delivery enable improved delivery efficiency to disease sites.[15–21] Recently, several studies have shown that nanoparticle formulations can improve therapies to ischemic stroke,[22–25] but cellular locations of therapeutic delivery in the brain are not well defined. In the cerebral I/R, neutrophils adhere to activated endothelium *via* membrane adherent proteins, such as integrin β_2 on neutrophils and ICAM-1 expressed on endothelium.[26] Targeting inflamed endothelium in the brain may be a promising approach to manage I/R-induced inflammation to prevent tissue damage. Lipid mediators derived from omega-3 polyunsaturated fatty acids (PUFA) have been shown to enhance inflammation resolution in inflammatory diseases.[27, 28] Resolvins are classified to Resolvin D (RvD) and Resolvin E (RvE) derived from docosahexaenoic acid (DHA) and from eicosapentaenoic acid (EPA), respectively.[29] The studies show that Resolvin D2 (RvD2) can decrease leukocyte-endothelium interactions, reduce cytokine production, and mitigate bacterial burden in a mouse sepsis model.[30] In the mechanisms, RvD2 induces the generation of nitric oxide in endothelium for decreased neutrophil-endothelium interactions.[30] RvD2 also binds a G-protein coupled receptor (GPR18) on neutrophils to inhibit neutrophil infiltration and stimulate neutrophil apoptosis, thus accelerating inflammation resolution.[31] Resolvin D2 is prone to directly bind to plasma proteins, therefore its bioavailability is decreased after intravenous administration. Recently, we have generated nanovesicles from neutrophils and demonstrated that nanovesicles can target inflamed lung.[32] Because of current insufficient therapies to ischemic stroke, here we proposed neutrophil nanovesicles to deliver RvD2 to a stroke lesion for improved treatment.

We report on a drug delivery platform comprised of neutrophil-membrane-derived nanovesicles loaded with RvD2. The nanovesicle-based delivery system would specifically target inflamed brain endothelium during I/R, and deliver RvD2 to prevent neuroinflammation. To test this hypothesis, we have developed intravital microscopy to real time visualize the binding of nanovesicles to inflamed endothelium in the live mouse brain in the cerebral I/R model. We have shown the usefulness of our nanovesicles in preventing the mouse neurological damage during reperfusion therapy to ischemic stroke.

RESULTS AND DISCUSSION

Design of RvD2-loaded Neutrophil Nanovesicles Targeted to Inflamed Brain Endothelium.

In this study, HL-60 cells (human promyelocytic leukemia cells) are selected since they are like neutrophils after their differentiation.[33,34] Inspired by the binding of neutrophils to endothelium during stroke, we proposed to generate nanovesicles derived from differentiated HL-60 cells using nitrogen cavitation. Nitrogen cavitation is a physical force to rapidly disrupt cells to generate nanoscale cell membrane-formed vesicles. [35]

Figure 1 shows the design of neutrophil-derived nanovesicles for targeted delivery of RvD2 to brain in a cerebral I/R mouse model. HL-60 nanovesicles (HVs) were generated from differentiated HL-60 cells induced by dimethyl sulfoxide (DMSO). Nitrogen cavitation followed by a series of centrifugation was used to generate nano-sized membrane vesicles.[32] RvD2 was selected because it may incorporate into the lipid bilayer of nanovesicles due to the lipid structure of RvD2. We hypothesized that the homing of RvD2-loaded nanovesicles (RvD2-HVs) in stroke lesions could diminish inflammation responses (such as neutrophil infiltration and cytokine release), thus preventing brain damage to rescue neurological functions in therapies to ischemic stroke. To examine this hypothesis, we established intravital microscopy of the live mouse brain to visualize delivery of nanovesicles to inflamed endothelium during ischemic stroke.

Generation and Characterization of RvD2-loaded Nanovesicles.

After HL-60 cells were differentiated to neutrophil-like cells, the cell suspension was placed in a vessel under nitrogen cavitation to generate nanovesicles followed by a series of centrifugation.[32] We measured size and zeta potential of nanovesicles using dynamic light scattering. We found that nanovesicles were 190 nm in diameter and their polydispersity index (PDI) was 0.21. It is unlikely that the vesicular size was dependent on RvD2 loading (Figure 2A). To confirm the membrane structure of nanovesicles, we performed cryo-electron microscopy (cryo-EM) to visualize intact nanovesicles in suspension (Figure 2B). The result showed that a vesicle was made of a thin layer, whose thickness was same as that of cell membrane. The sizes of nanovesicles were studied in Hanks' Balanced Salt solution (HBSS) and in HBSS with 20% of fetal bovine serum (FBS) at room temperature, respectively (Figure S1). We observed that nanovesicles did not change their size in serum compared to those in HBSS, suggesting that nanovesicles may be stable *in vivo*. It is interesting to observe that the zeta potential of nanovesicles was −10.1 mV, but it increased to −14 mV after RvD2 was added to nanovesicles, implying that RvD2 may be incorporated in the lipid bilayer of nanovesicles (Figure 2C). In addition, the mass of RvD2 has been determined by mass spectrometry (MS) (Figure S2) after RvD2 was extracted from nanovesicles using ethanol. This is consistent with the zeta potential changes of nanovesicles after RvD2 was loaded. We measured RvD2 release from nanovesicles using high-performance liquid chromatography (HPLC) (Figure S3). The result (Figure 2D) showed that RvD2 was able to release from nanovesicles and almost 80% RvD2 was released in 24 h. Adding 20% FBS in the nanovesicle suspension did not change the RvD2 release rate, suggesting that RvD2 may tightly be incorporated in nanovesicles when they are used for *in vivo* studies. Collectively, our results show that we have successfully generated nanovesicles

from cell membrane of HL-60 cells and have loaded the therapeutics in nanovesicles. In addition, nanovesicles are very stable with 20% of serum, implying that the nanovesicles may be good carriers for drug delivery.

Surface Proteins of Nanovesicles and Their Binding to Inflamed Endothelium.

Next, we determined whether nanovesicles had the similar membrane proteins to their parent cells. Since interactions between neutrophils and endothelial cells are mainly regulated by cell membrane proteins,[36] we have studied four major surface proteins, including integrin β_2, platelet endothelial cell adhesion molecule-1 (PECAM-1), P-selectin glycoprotein ligand-1 (PSGL-1), and integrin $\alpha_4\beta_1$ (VLA-4) (Figure 3A). Figure 3B shows the quantification of proteins in nanovesicles made from differentiated HL-60 cells (HVs), naïve HL-60 cells (NVs) (non-differentiated), and differentiated HL-60 cell lysis. It was found that the expression of integrin β_2 and PSGL-1 was increased by 2 and 7 folds in HVs, compared to those of NVs, respectively. These two proteins are required to facilitate the binding of neutrophils to inflamed endothelium.[37] The increased integrin β_2 and PSGL-1 in HVs were associated with the features of activated neutrophils after HL-60 cells were differentiated. Compared to the resource cells, the expression of integrin β_2 and PSGL-1 was dramatically increased in nanovesicles, while the intracellular (GAPDH) marker was decreased (Figure 3A) when we loaded the same amount of proteins for Western blot experiments. The result shows that nanovesicles contained less intracellular proteins after nitrogen cavitation, suggesting that our nanovesicles may be good drug carriers, consistent with the cryo-TEM image of nanovesicles (Figure 2B).

To determine the binding of nanovesicles to inflamed endothelium, we first investigated whether ICAM-1, a ligand of integrin β_2, was upregulated after human umbilical vein cells (HUVECs) were activated. The upregulation of ICAM-1 was observed 3 h after HUVECs were treated with TNF-α (100 ng/ml) (Fig. 3C). Confocal laser scanning microscopic images (Figure 3D) showed the interaction between nanovesicles and HUVECs after their co-culture. After we incubated DiO (Benzoxazolium, 3-octadecyl-2-[3-(3-octadecyl-2(3H)-benzoxazolylidene)-1-propenyl]-, perchlorate 34215–57-1)-fluorescently-labeled differentiated nanovesicles (HVs) with TNF-α-treated HUVECs, we imaged HUVECs, finding strong green fluorescence of HVs around the nuclei. In the control experiments, we incubated DiO-labeled non-differentiated nanovesicles (NVs) with TNF-α-treated HUVECs or incubated DiO-labeled HVs with normal HUVECs. In both cases, we observed weak fluorescence from nanovesicles, suggesting that the interaction between nanovesicles and HUVECs requires the adhesion molecules expressed on neutrophils and endothelium. To quantitatively analyze the interaction, we collected HUVECs to perform flow cytometry (Figure S4). The result is consistent with confocal fluorescence images (Figure 3D). Together, we demonstrate that HVs possess the membrane proteins of their parent cells required for binding to activated endothelial cells.

Nanovesicles Bind to Brain Endothelium in Cerebral I/R Model.

To address whether nanovesicles can target injured brain in stroke, we established the middle cerebral artery occlusion (MCAO) mouse model to mimic I/R injury in ischemic stroke. Lipid dye DiR (1,1'-Dioctadecyl-3,3,3',3'-tetramethylindotricarbocyanine iodide) was used

to label nanovesicles since DiR emits the light in near infrared and can be incorporated in the bilayer of nanovesicles.[32] Ischemia/reperfusion in the brain was performed in a mouse by inserting a monofilament to the middle cerebral artery, and 1 h later, the monofilament was withdrawn to restore the circulation (reperfusion). 1 h after reperfusion, we intravenously (i.v.) administered nanovesicles to the mouse. 1h and 11h after the injection, the mouse brain was imaged using *in vivo* imaging system (IVIS) (Figure 4A). The results showed that injured brain (the right brain) had a higher fluorescent intensity when DiR-labeled nanovesicles (DiR-HVs) were administered compared to the controls (free DiR in MCAO mice, DiR-labeled non-differentiated nanovesicles (DiR-NVs) in MCAO mice, and DiR-HVs in sham mice), indicating increased accumulation of HVs in the damaged brain. To quantitatively measure the accumulation of nanovesicles in the brain, we homogenized the left brain (no damage from MCAO surgery) and right brain (damage from MCAO surgery), respectively. The results (Figure 4B) showed that the fluorescence signals of dye molecules in the left brain were similar after administering free fluorescent dyes and fluorescently-labeled nanovesicles, indicating that nanovesicles did not selectively target non-damaged brain tissues. In contrast, the right brain tissues showed the different trafficking of nanovesicles. We observed that fluorescence of DiR-HVs significantly increased compared to that of DiR-NVs, and the fluorescence of DiR-HVs was not decreased in 11 h, which indicates that DiR-HVs can sustain in injured brain for several hours. Therefore, nanovesicles can efficiently deliver therapeutics to stroke lesions to improve therapeutic outcomes. When DiR-HVs were administered to sham mice, we observed that the fluorescence signal in the right brain was markedly diminished compared to that in MCAO mice. The results clearly indicate that HVs can selectively target injured brain tissues *via* adhesion proteins on HVs to facilitate their accumulation in inflamed brain. These data are consistent with the western blot results (Figure 3A and B), where the high expression of adhesion proteins on HVs required for binding to activated endothelium.

Furthermore, we studied the tissue deposition of nanovesicles in several organs using IVIS and also quantitatively measured fluorescence of dyes after tissues were homogenized (Figure S5). Although liver and spleen took up many nanovesicles, we still observed the marked nanovesicles in brain tissues. Collectively, the result indicates that trafficking of nanovesicles strongly depends on damaged brain tissues. Although we have shown that HVs accumulated in damaged brain (Figure 4A and 4B), it is not clear what cells interact with nanovesicles. To address this question, we established a cranial window to real time visualize trafficking of nanovesicles in a live mouse brain. Cranial window allows to image live brain microvasculature.[38] In the study, the partial mouse skull was removed, and a coverslip was applied on the damaged brain one week before the MCAO surgery. The mouse was placed in a special holder to reduce mouse movements during confocal microscopy (Figure 4C). The photograph of cranial window showed the intact brain vasculature under the cranial window (Figure 4C). 1 h after reperfusion, we i.v. injected BSA-Cy5 to fluorescently label blood vessels. Subsequently, nanovesicles fluorescently labeled with Dil ((1,1'-Dioctadecyl-3,3,3',3'-Tetramethylindocarbocyanine Perchlorate) (Dil-HVs) were i.v. injected into the mouse. It was observed that initially Dil-HVs (red) circulated, and then they were adherent to inflamed brain blood vessel (the top panel of Figure 4D and its video as shown in Movie 1). However, neither Dil-labeled non-differentiated nanovesicles (Dil-NVs)

in MCAO model (the middle panel of Figure 4D and its video as shown in Movie 2) nor Dil-HVs in healthy mice (the bottom panel of Figure 4D and its video as shown in Movie 3) were observed to bind to the brain vasculature. Compared with the traditional *ex vivo* brain straining, intravital microscopy offers the clear evidence of how nanovesicles interact with brain vasculature during ischemic stroke. Together, the results demonstrate that our nanovesicles could specifically target to inflamed endothelium in the brain, thus providing a tool to deliver therapeutics to stroke lesions.

RvD2-loaded Nanovesicles Diminish Neutrophil Infiltration in the Brain

Cytotoxicity of nanovesicles was examined before we asked whether we can exploit nanovesicles to deliver therapeutics to the brain. Normal human fibroblasts (NHFs) were incubated with HVs and RvD2-HVs for 24 h and 48 h respectively, and cell viability was examined using cell counting kit-8 (CCK-8) assay. We observed the high cell viability of NHFs after they were incubated with nanovesicles (Figure S6), showing that nanovesicles are not toxic when they are used for therapies since nanovesicle doses used in the MCAO mouse model were much lower than 100 mg/L.

Neutrophil infiltration plays a central role in stroke, so inhibiting neutrophil brain infiltration is a means to prevent secondary tissue damage during stroke treatment. Here, we addressed whether RvD2-loaded nanovesicles (RvD2-HVs) can inhibit neutrophil infiltration. We first used intravital microscopy to image neutrophil trafficking in the mouse brain in MCAO model. 3 h after reperfusion, BSA-Cy5 and Alexa Fluor 488 anti-mouse Ly-6G antibody were intravenously injected to mark blood vessels and neutrophils, respectively. We observed that neutrophils moved slowly in bloodstream, and a large number of neutrophils appeared outside of the brain vasculature (Figure 5A, and Movie 4 shows a 3D image taken by intravital microscopy). When RvD2-HVs were i.v. administered 1 h after reperfusion in the MCAO model, 2 h later we injected BSA-Cy5 and Alexa Fluor 488 anti-mouse Ly-6G antibody, and we found that neutrophil infiltration was dramatically decreased (Figure 5B, and Movie 5 shows a 3D image taken by intravital microscopy). Quantification of intravital microscopic images showed that RvD2-HVs decreased neutrophil infiltration by 10 folds compared to that without treatment (Figure 5C). The result indicates that RvD2-HVs can inhibit neutrophil infiltration in the mouse brain after reperfusion in ischemic stroke.

Furthermore, we studied the effect of RvD2-loaded nanovesicles on migration of human neutrophils using transmigration assay to mimic neutrophil transmigration *in vivo*. Human neutrophils were isolated from human donors, and 1×10^5 neutrophils were used per assay. In the normal condition (without any cytokine or chemokine added), neutrophils showed the low permeability to a monolayer of endothelial cells as 5% neutrophils were observed in the lower chamber. When 100 U of TNF-α and 10 nM of fMLP were added in the lower chamber, 89% neutrophils migrated to the lower chamber. After the treatment with RvD2-HVs (with 1nM RvD2), we observed a dramatic reduction of neutrophil transmigration to 26% (Figure 5D). We also observed that free RvD2 (1nM) showed the decrease of neutrophil transmigration (Figure 5D), implying that RvD2 regulates neutrophil movements. Interestingly, we observed that HVs alone can also prevent neutrophil transmigration, but the effect was not significant. The binding of HVs to endothelium may inhibit neutrophil

adhesion to endothelium for transmigration. Collectively, both *in vitro* and *in vivo* experiments demonstrate that the binding of RvD2-HVs to inflamed endothelium enhances the delivery of RvD2 in the brain to prevent neutrophil infiltration in ischemic stroke lesions.

RvD2-loaded Nanovesicles Increase Inflammation Resolution in MCAO Model

Next, we addressed whether RvD2-loaded nanovesicles increased inflammation resolution in ischemic stroke. We measured myeloperoxidase (MPO) activity in the brain, a marker of neutrophil tissue infiltration.[39] Mice were administered with therapeutics 1 h after reperfusion in the ischemic mouse. Brain tissues were obtained 22 h after administration of therapeutics for inflammation analysis. We found that RvD2-HVs dramatically reduced MPO content compared to several controls (free HVs, free RvD2 and RvD2-NVs) (Figure 6A). In addition, we analyzed the expression of ICAM-1 in inflamed brain in the MCAO model using Western blot. The result showed that the expression of ICAM-1 in brain increased in MCAO mice. However, the treatment with RvD2-HVs inhibited ICAM-1 expression in the damaged brain 3h after administration of therapeutics (Figure S7). The results indicate that RvD2-HVs can regulate both neutrophils and endothelium in the brain. To better elucidate the neuroprotective effect of RvD2-HVs in I/R injury, pro-inflammatory cytokines including TNF-α, IL-6 and IL-1β were assessed because cytokines play a central role in neuroinflammation and causes brain damage. ELISA (enzyme-linked immunosorbent assay) results showed that RvD2-loaded nanovesicles diminished all the three cytokines in the injured half brain (Fig. 6B-D) compared to several controls. Our results indicate that RvD2-loaded nanovesicles can enhance delivery of RvD2 in inflamed brain caused by I/R, thus mitigating neuroinflammation.

RvD2-loaded Nanovesicles Protect Brain Injury Induced by Stroke

Reperfusion therapy to ischemic stroke is to restore circulation in the brain, but it spontaneously activates inflammation pathways that may damage brain tissues. Here, we asked whether RvD2-loaded nanovesicles can protect the brain damage and improve mouse neurological functions after stroke. The brain was sliced 22 h after the treatment with several formulations, and the brain slices were stained using 1% triphenyltetrazolium chloride (TTC) solution to quantify infarcted brain tissues (Figure 7A, and a full panel of brain sections as shown in Figure S8). TTC is a redox indicator to differentiate dead and living tissues. It is enzymatically reduced to show red color in normal tissues, but it remains white color in an area of necrotic tissues.[40] The normal brain tissues showed red, but the I/R injured brain showed pale color, indicating that MCAO damaged brain tissues. When mice were treated with RvD2-HVs, the brain tissues (left side of the image) injured due to MCAO showed red similar as that of sham mice. The result indicates that RvD2-HVs prevented the infarction formation in the brain during MCAO. Quantification of infarcted brain using ImageJ showed that RvD2-HVs decreased the infarct volume to 16% compared to 46% when the mouse was treated with PBS treatment (Figure 7B). Compared to RvD2-NVs, RvD2-HVs still showed the significant reduction of infarct volume, suggesting that targeted delivery of RvD2 using HVs showed more benefit. Furthermore, mouse neurological deficit scores were recorded (the videos shown in Movie 6–11). The scores were given by two independent people following the instructions adopted from Bederson,[41,42] and the average scores were shown in Figure 7C. Treatment with RvD2-HVs significantly ameliorated

neurological deficit induced by I/R compared to free nanovesicles, free RvD2 and RvD2-NVs. The results indicate that specifically delivering RvD2 to the mouse brain using our nanovesicles combined to reperfusion therapy of ischemic brain can improve current stroke treatments.

We have shown that neutrophil-membrane-derived nanovesicles can specifically target inflamed brain endothelium during I/R, and this process is regulated by adhesion molecules expressed on neutrophil membrane. We found that integrin β_2 and PSGL-1 are highly expressed on nanovesicles, and they facilitate the binding of nanovesicles to inflamed endothelium. Liposomes can be loaded with a wide range of drugs and they have been tested in clinic,[43] thus it is possible that membrane adhesion molecules discovered in our nanovesicles may be linked to liposome surfaces to target activated endothelium. But incorporating cell membrane proteins to liposomes may be challenging because controlling the orientation of proteins is required to bind inflamed endothelium. In addition, our nanovesicles are directly derived from cells, so the nanovesicles have the natural features that liposomes do not possess. We expect that our nanovesicles would be better than bio-functionalized liposomes in nanomedicine, but the reproducibility and quality of nanovesicles should be considered when they are used in clinic.

CONCLUSION

Here, we report on a drug delivery system made from neutrophil nanovesicles that can specifically target inflamed brain endothelium in ischemic stroke mouse model. Our approach is inspired by the interaction between neutrophils and brain endothelium occurred in the pathogenesis of ischemic stroke. We proposed neutrophil membrane-formed nanovesicles containing their parent cell properties may facilitate the delivery of therapeutics to stroke tissues. We have demonstrated this concept using HL-60 cell membrane-derived nanovesicles that can specifically target inflamed brain vasculature and deliver RvD2, thus enhancing resolution of inflammation during ischemic stroke therapy. Most importantly, we have established intravital microscopy of the live mouse brain to real time visualize the binding of neutrophil-derived nanovesicles to inflamed vasculature during reperfusion therapy to ischemic stroke. Compared to conventional brain imaging (such as magnetic resonance imaging), our intravital microscopy is a powerful tool to image subcellular locations of nanotherapeutics in diseased tissues. Most strokes are related to ischemic brain, and reperfusion is a major means to treat ischemic stroke by restoration of blood flow in the brain, but it causes neuroinflammation. We have shown that our nanovesicles can deliver RvD2 to resolve neuroinflammation. Combining this nanovesicle delivery system with current stroke therapies may be a synergistic approach to improve patient outcomes. Furthermore, neutrophils are the most abundant white blood cells in humans, therefore, our nanovesicles made from neutrophils could be potential in developing personalized nanomedicine in clinic to treat various inflammation-related diseases.

MATERIALS AND METHODS

Biological and Chemical Agents:

Human HL-60 cell lines were obtained from ATCC (Manassas, VA, Catalog No. CCL-240). Human umbilical vein endothelial cells (HUVECs, Catalog No. CC-2517) were obtained from Lonza (Walkersville, MD). Resolvin D2 was purchased from Cayman Chemical (Michigan, MI, Catalog No. 10007279). Anti-ICAM-1 antibody (Catalog No. sc-390483), anti-integrin-β_2 antibody (Catalog No. sc-393790), anti-PECAM-1 antibody (Catalog No. sc-376764), anti-VLA-4 antibody (Catalog No. sc-365569), anti-PSGL-1 antibody (Catalog No. sc-13535) were purchased from Santa Cruz Biotechnology (Santa Cruz, CA). Dil (3 H-Indolium, 2-(3-(1,3-dihydro- 3,3-dimethyl-1-octadecyl-2 H-indol-2-ylidene)-1-propenyl)-3,3-dimethyl-1-octadecyl-, perchlorate) [(Ex(549 nm)\Em(565 nm)] (Catalog No. D282), DiR (1,1'-Dioctadecyl-3,3,3',3'-Tetramethylindotricarbocyanine Iodide) [Ex(750 nm)\Em(780 nm)] (Catalog No. D12731), DAPI (4,6-diamidino-2-phenylindole) (Catalog No. P36931), Penicillin streptomycin (pen strep, Catalog No. 15140–122) and glutamine (100×) (Catalog No. 25030–081) were purchased from Life Technologies (Grand Island, NY). Recombinant human TNF-α (Catalog No. 570109), Alexa Fluor 488 anti-mouse Ly-6G antibody (Catalog No. 127626) and ELISA kits for TNF-α (Catalog No. 430904), IL-6 (Catalog No. 431304) and IL-1β (Catalog No. 432604) were purchased from Biolegend (San Diego, CA). 2,3,5-Triphenyltetrazolium chloride and o-Dianisidine dihydrochloride were purchased from Sigma-Aldrich (St. Louis, MO, Catalog No. D3252–5G).

Preparation and Characterization of Membrane-derived Nanovesicles.

Human HL-60 cells were cultured in RPMI1640 with 10% (v/v) FBS and 1% (v/v) pen strep/glutamine. To differentiate HL-60 cells, 1.25% (v/v) DMSO were added in the medium and cells were cultured for 4–6 days.[44] Differentiated HL-60 cells were re-suspended in HBSS, and then nitrogen cavitation at a pressure of 350–400 psi was used to disrupt cells. The resulting suspension was centrifuged at 2,000 g for 30 min to remove nuclei. The supernatant was centrifuged at 100,000 g for 30 min to obtain nanovesicles, and this process was repeated twice. Nanovesicles were lyophilized and stored at −20°C for future use. Nanovesicles were imaged using cryo-electron microscopy (cryo-EM). Particle size and zeta potential of nanovesicles and RvD2-vesicles were measured using Malvern Zetasizer Nano ZS90 (Westborough, MA).

Preparation of RvD2-loaded and DiI/DiO/DiR-labeled Nanovesicles.

Nanovesicle suspensions were heated to 37°C and the pH value was adjusted to 4.5 for drug loading. RvD2 and nanovesicles were quickly mixed at a ratio of 2 μg (RvD2)/ml and 200 μg/mL of nanovesicles, followed by sonication for 2 min on ice, and incubated at 37 °C for 30 min. The suspension was centrifuged at 100,000 g to remove free RvD2. Finally, the RvD2 loading efficiency was 10% determined by HPLC. In the release study, prepared RvD2-HVs were equally divided in several tubes, and at different time points, the samples were centrifuged at 100,000 g to obtain the pellets. Then ethanol was used to extract RvD2 from the pellets. Extracted RvD2 was analyzed by mass spectrometry (MS) and high performance liquid chromatography (HPLC). In HPLC experiment, the mobile phase

(methanol:water:acetic acid = 62:38:0.01) was used at a flow rate of 1.0 ml/min.[31] The fluorescent labeling method was similar as the preparation of RvD2-loaded nanovesicles. Nanovesicle suspensions were heated to 37°C. Dil/DiO/DiR and nanovesicles were quickly mixed at a ratio of 100 mM (Dil/DiO/DiR) and 4 mg nanovesicles, followed by sonication for 2 min on ice, and incubated at 37 °C for 30 min. The suspension was centrifuged at 100,000 g to remove free Dil/DiO/DiR.

Western Blot.

Differentiated HL-60 cell lysis, non-differentiated nanovesicles and differentiated nanovesicles were studied using western blot. Integrin β_2, platelet endothelial cell adhesion molecule (PECAM-1), P-selectin glycoprotein ligand-1 (PSGL-1) and integrin α4 (VLA-4) were studied using western blot. Quantification of western blots was performed relative to GAPDH using Bio-Rad image analysis software.

Culture of Human Umbilical Vein Endothelial Cells (HUVECs).

HUVECs were cultured in EBM medium supplemented with a commercial kit including FBS, rhEGF, hydrocortisone, GA-100, bovine brain extract, and ascorbic acid. 100 ng/ml of tumor necrosis factor-α (TNF-α) was added to the cells and 3 h later, ICAM-1 expression was determined by Western blot.

In vitro Binding of Nanovesicles to Inflamed Endothelium.

1.5×10^5/well of HUVECs were seeded on a cover slip in a small dish. After the treatment of TNF-α, 60 μl of DiO-labeled nanovesicles (2 mg/ml) were added into each well and incubated for 30 min at 37ºC under continuous agitation to mimic *in vivo* conditions. Cells were washed twice with PBS and fixed with 4% PFA for 20 min on ice. Next, the mounting reagent containing DAPI (4',6-diamidino-2-phenylindole) was added to the cells, and they were imaged using a confocal microscope (Nikon A1R+).

Cytotoxicity Assessment *in vitro.*

Human normal fibroblasts (NHFs) were cultured in DMEM medium with 10% (v/v) FBS and 1% (v/v) pen strep/glutamine. Cells were cultured in 96-well plates for 24 h to reach a confluence of 90%. Then, the medium was changed with fresh medium containing HVs or RvD2-HVs at different HVs concentrations (0, 1, 5, 10 and 100 mg/L). At 24 h or 48 h, 10 μL of CCK-8 solutions were added to each well and incubated for 2 h. The absorbance of formazan was measured at 450 nm by microplate reader.

Cranial Window.

All animal experiments have been approved by the Institutional Animal Care and Use Committee (IACUC) in Washington State University. C57 mice were anesthetized by intraperitoneal injection of a mixture of 100 mg/kg ketamine and 5 mg/kg xylazine. The mouse body temperature was maintained at 37°C throughout the experiment. The fur was shaved on the top of a head, and the skin was disinfected with iodine and 75% ethanol. A dorsal midline incision was made to expose the skull. The skull surface was treated with a bonding agent and binding glue. A high-speed drill was used to drill a circle area to remove

the skull bone on the right brain. The exposed brain was moistened with saline throughout the experiment. A 3 mm (diameter) glass window was placed onto the circle area, and a super glue was used to hold the glass.[45] In the final step, a bar was mounted on the head for intravital microscopy. After the experiment, the mouse was individually caged and treated with a mixture of buprenorphine and antibiotics for pain relief and anti-infection. 7 days after recovery from the surgery, mice were imaged using an intravital microscope (Nikon $A1R^+$ laser confocal microscope with a resonant scanner).

Middle Cerebral Artery Occlusion (MCAO) Model.

All animal experiments have been approved by IACUC. Male C57 mice (24–28 g) were used following the previous studies.[46] Mice were anesthetized by intraperitoneal injection of 100 mg/kg of ketamine and 5mg/kg of xylazine. They were positioned on a heating pad in the supine position. The skin was disinfected with iodine and 75% ethanol. A midline neck incision was made to expose a carotid artery (CA). The external carotid artery (ECA) was then separated and occluded with two knots. Next, the internal carotid artery (ICA) was isolated, and the CA and ICA were clipped by microvascular clip. A small hole was cut in ECA between a knot and the bifurcation point. A silicon rubber-coated 6–0 medium MCAO suture was then introduced into ICA, until it stops at the clip. The clipped arteries were opened while the suture was inserted to occlude the vessel. The third knot on RICA was closed to hold the suture in position. The mouse was kept for 60 min after occlusion in a heated cage and the wound was closed with a small suture clip. The third knot was loosened and the filament was withdrawn for reperfusion. Finally, the skin was closed and the mouse was returned to an individual cage.

Ex vivo Brain and Other Organs Imaging and Quantification.

Mouse brain tissues (left and right brain tissues), and other organs (heart, spleen, lung, kidney and liver) were collected at 1h and 11h post-injection of free DiR dye, DiR-labeled HVs and DiR-labeled NVs after MCAO surgery, and DiR-labeled HVs in sham groups. The tissues were imaged under *in vivo* imaging system (IVIS). Afterwards, tissues were collected and homogenate in PBS buffer, and fluorescent signals of DiR were measured by a microplate reader.

In vivo Real-time Imaging of Nanovesicles in I/R Mice.

Cranial window was first placed on the mouse right brain. At least 7 days after the operation, intravital microscopy was performed using a Nikon $A1R^+$ laser scanning confocal microscope with a water immersion objective (20x) and 4 lasers (4005nm/488nm/560nm/640nm) from Coherent. MCAO was performed on the mouse with a cranial window. Ischemia was operated on right artery to induce the injury in the right brain. 1 h later, the mouse was re-perfused after the filament in the artery was withdrawn. Fluorescently labeled-nanovesicles were administrated 1h after reperfusion. Half an hour later, BSA-Cy5 was i.v. injected to label bloodstream, and circulating and binding of nanovesicles were observed using intravital microscopy. A healthy mouse (without I/R) was used as control. During imaging, all mice were under anesthesia with 100 mg/kg of ketamine and 5mg/kg of xylazine, on a heating pad.

In vivo Real-time Imaging of Neutrophils in I/R Mice.

Cranial window was first placed on a mouse head. At least 7 days after the surgery, intravital microscopy was performed. MCAO was performed on the mouse with a cranial window. RvD2-nanovesicles or PBS buffer (as a control) were administrated 1h after reperfusion. 2 h later, BSA-Cy5 and Alexa Fluor 488 anti-mouse Ly-6G antibody were administrated to label bloodstream and neutrophils, respectively. Neutrophil trafficking was observed in the brain using intravital microscopy. During imaging, all mice were under anesthesia with 100 mg/kg of ketamine and 5mg/kg of xylazine, on a heating pad.

Human Neutrophil Isolation.

Institutional review board (IRB) in Washington State University has approved our protocol to use human neutrophils. Human blood was obtained from volunteers following the signed consent. Polymorphonuclear leukocytes (PMNs) were isolated using a density gradient technique.[47] Whole blood was carefully added into a mixture of Histopaque-1077 and Histopaque-1119. Samples were centrifuged at 900 g for 30 min at room temperature. The upper layer was carefully aspirated to the opaque interface that contains mononuclear cells. The opaque interface was carefully transferred into a clean tube. The cells were washed by 10 mL of phosphate buffered saline (PBS). In the final step, the cells were centrifuged at 250 g for 10 min, re-suspended in RPMI-1640 media supplemented with 10% FBS (v/v), counted, and incubated at room temperature until use.

Transmigration Assay.

The experiment was performed following the previously established method.[48] Transwell plates with pores of 3-μm in diameter, 12-mm diameter membrane was first coated with fibronectin for 2 h at room temperature. HUVECs were added (1×10^5 cells/well) to transwells and cultured in a 24-well plate overnight until 95% confluence. Prior to transmigration assays, a HUVEC monolayer was pretreated with 100 ng/ml TNF-α for 3h to activate HUVECs. Six groups were investigated: 1) No cytokines or chemokines added in the lower chamber. 2) Treatment with PBS buffer. 3) Treatment with nanovesicles only (40 μg/assay). 4) Treatment with RvD2 only (1nM). 5) Treatment with RvD2-NVs (with 1nM RvD2). 6) Treatment with RvD2-HVs (with 1nM RvD2). Cytokines and chemokines were added to the bottom well in groups 2, 3, 4, 5 and 6, with 100U of TNF-α and 10nM of N-formyl-methionyl-leucyl-phenylalanine (fMLP) in 0.6 mL of cell culture medium as the chemo-attractants. Human neutrophils (1×10^5 cells/well) were placed in the upper transwell chamber. Transmigration assay was performed for 3 h at 37°C. Neutrophils were collected from the top and bottom chambers and gently washed with PBS buffer for cell counting.

Myeloperoxidase (MPO) Activity and Cytokine Levels.

Mouse brains were collected at 22 h post-injection of therapeutics (24 h after MCAO surgery) in MCAO model. They were weighed and homogenized in 50mM potassium phosphate buffer containing 5% hexadecyltrimethylammonium bromide (HTAB). The homogenate was sonicated three times for 1 min on ice, and centrifuged at 10,000 rpm for 10 min at 4°C. Next, 10 μL of the supernatant was loaded into each well of a 96-well plate. A solution of o-Dianisidine dihydrochloride with 0.0005% hydrogen peroxide in 190 μL of

potassium phosphate buffer was added to the samples. Absorbance was measured at 450 nm every 1 minute for 3 minutes. MPO activity was expressed as a change in absorbance per minute per gram of tissue.[49] Cytokines (TNF-α, IL-1β and IL-6) were quantified in brain homogenate (in PBS buffer) using commercial ELISA kits as three replicates.

ICAM-1 Expression in Brain.

Mouse brain tissues were collected at 3 h post-injection of therapeutics (5 h after MCAO surgery). They were weighed and homogenized in PBS buffer. ICAM-1 expression was analyzed using western blot.

Assessment of I/R injury by Neurological Deficit and Infarct Volume.

Mouse neurological functions were measured based on mouse behaviors after analysis of videos taken at 22 h post-injection of therapeutics (24 h after MCAO surgery) in MCAO model. The neurological deficit scores were recorded blindly by two people. The scores were divided to five grades: Grade 0: normal and no neurological defect; Grade 1: mild circling movements when picked up by a mouse tail, and attempts to rotate to the contralateral side; Grade 2: consistent strong and immediate circling, or an animal only turned to the surgery contralateral side while the animal was suspended by holding the tail; Grade 3: severe rotation progressing into loss of walking or righting reflex; Grade 4: an animal did not walk spontaneously and had some degree of consciousness. In addition, mouse brains were collected and sectioned into 2 mm-thick coronal slices. Slices was stained with 1% of 2, 3, 5-triphenyltetrazolium chloride (TTC) at 37ºC for 30 min. TTC-stained sections was photographed and the digital images were analyzed using ImageJ. The percentage of infarction (infarct ratio) was calculated using the following formula: Infarct ratio (%) = infarct volume (mm^3) / total coronal section (mm^3) x100%.[50]

Statistical Analysis.

Student's t-test or two-way analysis of variance (ANOVA) were performed to analyze data using GraphPad Prism 6.0. Values were expressed as means ± SD and $p < 0.05$ is considered statistically significant.

Supplementary Material

Refer to Web version on PubMed Central for supplementary material.

ACKNOWLEDGMENTS

This work was supported by NIH grant RO1GM116823 to Z.W.

REFERENCES

1. Collard CD; Gelman S Pathophysiology, Clinical Manifestations, and Prevention of Ischemia-Reperfusion Injury. Anesthesiology 2001, 94, 1133–1138. [PubMed: 11465607]
2. Strong K; Mathers C; Bonita R Preventing Stroke: Saving Lives around the World. Lancet Neurol. 2007, 6, 182–187. [PubMed: 17239805]
3. Lo EH; Dalkara T; Moskowitz MA Mechanisms, Challenges and Opportunities in Stroke. Nat Rev Neurosci. 2003, 4, 399–415. [PubMed: 12728267]

4. Becher B; Spath S; Goverman J Cytokine Networks in Neuroinflammation. Nat Rev Immunol. 2017, 17, 49–59. [PubMed: 27916979]
5. Iadecola C; Anrather J The Immunology of Stroke: From Mechanisms to Translation. Nat Med. 2011, 17, 796–808. [PubMed: 21738161]
6. Shichita T; Sakaguchi R; Suzuki M; Yoshimura A Post-Ischemic Inflammation in the Brain. Front Immunol. 2012, 3, 132. [PubMed: 22833743]
7. Pan J; Konstas AA; Bateman B; Ortolano GA; Pile-Spellman J Reperfusion Injury Following Cerebral Ischemia: Pathophysiology, Mr Imaging, and Potential Therapies. Neuroradiology 2007, 49, 93–102. [PubMed: 17177065]
8. Kalogeris T; Baines CP; Krenz M; Korthuis RJ Cell Biology of Ischemia/Reperfusion Injury. Int Rev Cell Mol Biol. 2012, 298, 229–317. [PubMed: 22878108]
9. Lakhan SE; Kirchgessner A; Hofer M Inflammatory Mechanisms in Ischemic Stroke: Therapeutic Approaches. J Transl Med. 2009, 7, 97. [PubMed: 19919699]
10. Gautier S; Ouk T; Petrault O; Caron J; Bordet R Neutrophils Contribute to Intracerebral Haemorrhages after Treatment with Recombinant Tissue Plasminogen Activator Following Cerebral Ischaemia. Br J Pharmacol. 2009, 156, 673–679. [PubMed: 19210512]
11. Khan MM; Motto DG; Lentz SR; Chauhan AK Adamts13 Reduces Vwf-Mediated Acute Inflammation Following Focal Cerebral Ischemia in Mice. J Thromb Haemost. 2012, 10, 1665–1671. [PubMed: 22712744]
12. Vinten-Johansen J Involvement of Neutrophils in the Pathogenesis of Lethal Myocardial Reperfusion Injury. Cardiovasc Res. 2004, 61, 481–497. [PubMed: 14962479]
13. Fulurija A; Ashman RB; Papadimitriou JM Neutrophil Depletion Increases Susceptibility to Systemic and Vaginal Candidiasis in Mice, and Reveals Differences between Brain and Kidney in Mechanisms of Host Resistance. Microbiology 1996, 142, 3487–3496. [PubMed: 9004511]
14. Jaeger BN; Donadieu J; Cognet C; Bernat C; Ordonez-Rueda D; Barlogis V; Mahlaoui N; Fenis A; Narni-Mancinelli E; Beaupain B; Bellanne-Chantelot C; Bajenoff M; Malissen B; Malissen M; Vivier E; Ugolini S Neutrophil Depletion Impairs Natural Killer Cell Maturation, Function, and Homeostasis. J Exp Med. 2012, 209, 565–580. [PubMed: 22393124]
15. Chu D; Dong X; Zhao Q; Gu J; Wang Z Photosensitization Priming of Tumor Microenvironments Improves Delivery of Nanotherapeutics via Neutrophil Infiltration. Adv Mater. 2017, 10.1002/adma.201701021.
16. Torchilin VP Multifunctional, Stimuli-Sensitive Nanoparticulate Systems for Drug Delivery. Nat Rev Drug Discov. 2014, 13, 813–827. [PubMed: 25287120]
17. Wang Z; Li J; Cho J; Malik AB Prevention of Vascular Inflammation by Nanoparticle Targeting of Adherent Neutrophils. Nat Nanotechnol. 2014, 9, 204–210. [PubMed: 24561355]
18. Wang Z; Tiruppathi C; Minshall RD; Malik AB Size and Dynamics of Caveolae Studied Using Nanoparticles in Living Endothelial Cells. ACS Nano 2009, 3, 4110–4116. [PubMed: 19919048]
19. Wang Z; Tiruppathi C; Cho J; Minshall RD; Malik AB Delivery of Nanoparticle: Complexed Drugs Across the Vascular Endothelial Barrier via Caveolae. IUBMB Life 2011, 63, 659–667. [PubMed: 21766412]
20. Chen H; Zhang W; Zhu G; Xie J; Chen X Rethinking Cancer Nanotheranostics. Nat Rev Mater. 2017, 10.1038/natrevmats.2017.24.
21. Du B; Jiang X; Das A; Zhou Q; Yu M; Jin R; Zheng J Glomerular Barrier Behaves as an Atomically Precise Bandpass Filter in a Sub-Nanometre Regime. Nat Nanotechnol. 2017, 12, 1096–1102. [PubMed: 28892099]
22. Lv W; Xu J; Wang X; Li X; Xu Q; Xin H Bioengineered Boronic Ester Modified Dextran Polymer Nanoparticles as Reactive Oxygen Species Responsive Nanocarrier for Ischemic Stroke Treatment. ACS Nano 2018, 10.1021/acsnano.8b00477.
23. Gaudin A; Yemisci M; Eroglu H; Lepetre-Mouelhi S; Turkoglu OF; Donmez-Demir B; Caban S; Sargon MF; Garcia-Argote S; Pieters G; Loreau O; Rousseau B; Tagit O; Hildebrandt N; Le Dantec Y; Mougin J; Valetti S; Chacun H; Nicolas V; Desmaele D; Andrieux K et al. Squalenoyl Adenosine Nanoparticles Provide Neuroprotection after Stroke and Spinal Cord Injury. Nat Nanotechnol. 2014, 9, 1054–1062. [PubMed: 25420034]

24. Tian T; Zhang HX; He CP; Fan S; Zhu YL; Qi C; Huang NP; Xiao ZD; Lu ZH; Tannous BA; Gao J Surface Functionalized Exosomes as Targeted Drug Delivery Vehicles for Cerebral Ischemia Therapy. Biomaterials 2018, 150, 137–149. [PubMed: 29040874]
25. Liu X; Ye M; An CY; Pan LQ; Ji LT The Effect of Cationic Albumin-Conjugated Pegylated Tanshinone Iia Nanoparticles on Neuronal Signal Pathways and Neuroprotection in Cerebral Ischemia. Biomaterials 2013, 34, 6893–6905. [PubMed: 23768781]
26. Kolaczkowska E; Kubes P Neutrophil Recruitment and Function in Health and Inflammation. Nat Rev Immunol. 2013, 13, 159–175. [PubMed: 23435331]
27. Gilroy DW; Lawrence T; Perretti M; Rossi AG Inflammatory Resolution: New Opportunities for Drug Discovery. Nat Rev Drug Discov. 2004, 3, 401–416. [PubMed: 15136788]
28. Serhan CN; Chiang N; Van Dyke TE Resolving Inflammation: Dual Anti-Inflammatory and Pro-Resolution Lipid Mediators. Nat Rev Immunol. 2008, 8, 349–361. [PubMed: 18437155]
29. Buckley CD; Gilroy DW; Serhan CN Proresolving Lipid Mediators and Mechanisms in the Resolution of Acute Inflammation. Immunity 2014, 40, 315–327. [PubMed: 24656045]
30. Spite M; Norling LV; Summers L; Yang R; Cooper D; Petasis NA; Flower RJ; Perretti M; Serhan CN Resolvin D2 Is a Potent Regulator of Leukocytes and Controls Microbial Sepsis. Nature 2009, 461, 1287–1291. [PubMed: 19865173]
31. Chiang N; Dalli J; Colas RA; Serhan CN Identification of Resolvin D2 Receptor Mediating Resolution of Infections and Organ Protection. J Exp Med. 2015, 212, 1203–1217. [PubMed: 26195725]
32. Gao J; Chu DF; Wang ZJ Cell Membrane-Formed Nanovesicles for Disease-Targeted Delivery. J Control Release 2016, 224, 208–216. [PubMed: 26778696]
33. Martin SJ; Bradley JG; Cotter TG Hl-60 Cells Induced to Differentiate Towards Neutrophils Subsequently Die via Apoptosis. Clin Exp Immunol. 1990, 79, 448–453. [PubMed: 2317949]
34. Gao J; Wang SH; Wang ZJ High Yield, Scalable and Remotely Drug-Loaded Neutrophil-Derived Extracellular Vesicles (Evs) for Anti-Inflammation Therapy. Biomaterials 2017, 135, 62–73. [PubMed: 28494264]
35. Wang S; Dong X; Gao J; Wang Z Targeting Inflammatory Vasculature by Extracellular Vesicles. AAPS J. 2018, 20, 37. [PubMed: 29484558]
36. Phillipson M; Kubes P The Neutrophil in Vascular Inflammation. Nat Med. 2011, 17, 1381–1390. [PubMed: 22064428]
37. Nauseef WM; Borregaard N Neutrophils at Work. Nat Immunol. 2014, 15, 602–611. [PubMed: 24940954]
38. Goldey GJ; Roumis DK; Glickfeld LL; Kerlin AM; Reid RC; Bonin V; Schafer DP; Andermann ML Removable Cranial Windows for Long-Term Imaging in Awake Mice. Nat Protoc. 2014, 9, 2515–2538. [PubMed: 25275789]
39. Feuerstein GZ Correlation between Myeloperoxidase-Quantified Neutrophil Accumulation and Ischemic Brain Injury in the Rat - Effects of Neutrophil Depletion - Comment. Stroke 1994, 25, 1475–1475.
40. Benedek A; Moricz K; Juranyi Z; Gigler G; Levay G; Harsing LG, Jr.; Matyus P; Szenasi G; Albert M Use of Ttc Staining for the Evaluation of Tissue Injury in the Early Phases of Reperfusion after Focal Cerebral Ischemia in Rats. Brain Res. 2006, 1116, 159–165. [PubMed: 16952339]
41. Bederson JB; Pitts LH; Tsuji M; Nishimura MC; Davis RL; Bartkowski H Rat Middle Cerebral-Artery Occlusion - Evaluation of the Model and Development of a Neurologic Examination. Stroke 1986, 17, 472–476. [PubMed: 3715945]
42. Schaar KL; Brenneman MM; Savitz SI Functional Assessments in the Rodent Stroke Model. Exp Transl Stroke Med. 2010, 2, 13. [PubMed: 20642841]
43. Zucker D; Marcus D; Barenholz Y; Goldblum A Liposome Drugs' Loading Efficiency: A Working Model Based on Loading Conditions and Drug's Physicochemical Properties. J Control Release 2009, 139, 73–80. [PubMed: 19508880]
44. Tarella C; Ferrero D; Gallo E; Pagliardi GL; Ruscetti FW Induction of Differentiation of Hl-60 Cells by Dimethyl Sulfoxide: Evidence for a Stochastic Model Not Linked to the Cell Division Cycle. Cancer Res. 1982, 42, 445–449. [PubMed: 6948604]

45. Mostany R; Portera-Cailliau C A Craniotomy Surgery Procedure for Chronic Brain Imaging. J Vis Exp. 2008, 10.3791/680.

46. Belayev L; Alonso OF; Busto R; Zhao W; Ginsberg MD Middle Cerebral Artery Occlusion in the Rat by Intraluminal Suture. Neurological and Pathological Evaluation of an Improved Model. Stroke 1996, 27, 1616–1622. [PubMed: 8784138]

47. Nauseef WM Isolation of Human Neutrophils from Venous Blood. Methods Mol Biol. 2014, 1124, 13–18. [PubMed: 24504943]

48. Zhao Y; Jiang Y; Lv W; Wang ZY; Lv LY; Wang BY; Liu X; Liu Y; Hu QY; Sun WJ; Xu QW; Xin HL; Gu Z Dual Targeted Nanocarrier for Brain Ischemic Stroke Treatment. J Control Release 2016, 233, 64–71. [PubMed: 27142584]

49. Pulli B; Ali M; Forghani R; Schob S; Hsieh KLC; Wojtkiewicz G; Linnoila JJ; Chen JW Measuring Myeloperoxidase Activity in Biological Samples. PloS On. 2013, 10.1371/journal.pone.0067976.

50. Liu X; An C; Jin P; Liu X; Wang L Protective Effects of Cationic Bovine Serum Albumin-Conjugated Pegylated Tanshinone Iia Nanoparticles on Cerebral Ischemia. Biomaterials 2013, 34, 817–830. [PubMed: 23111336]

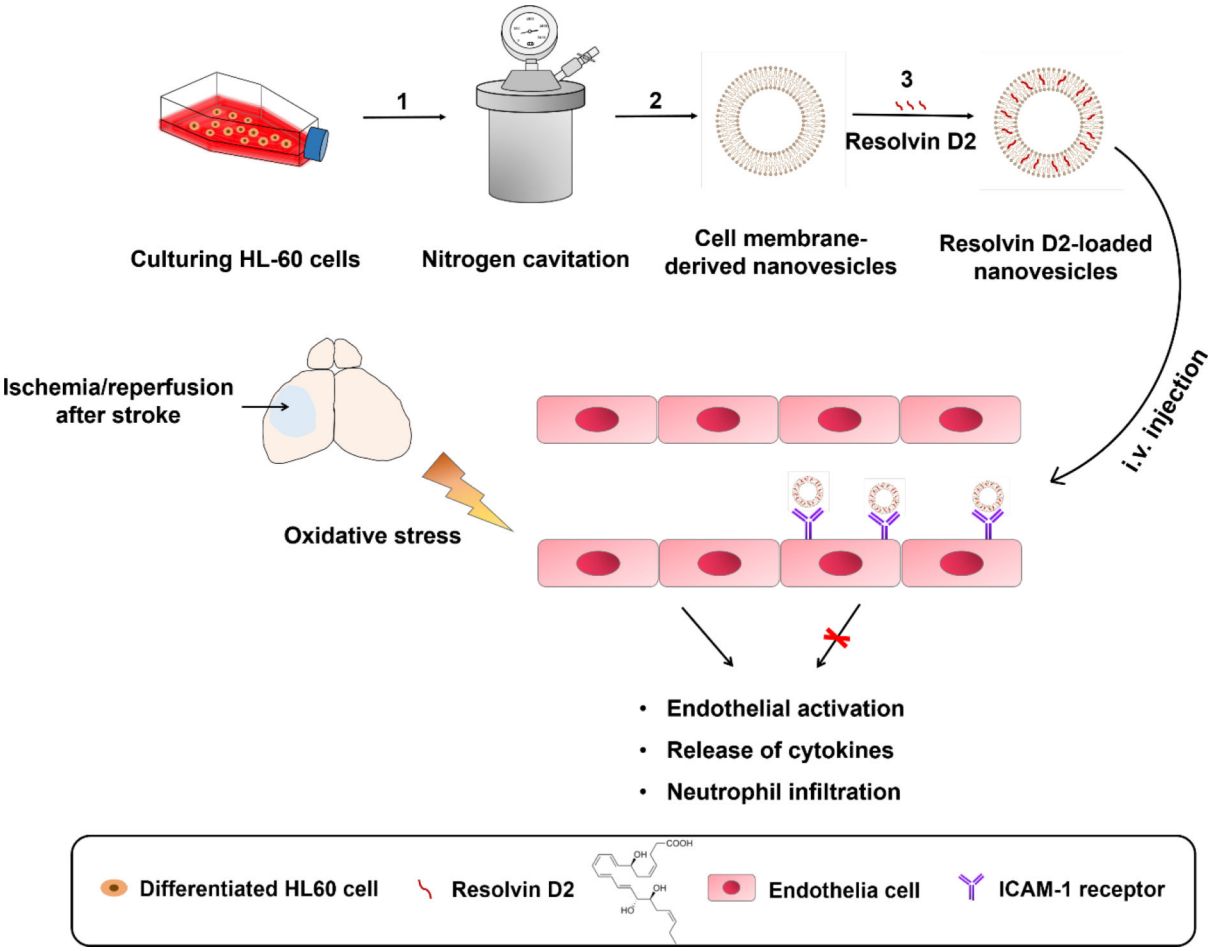

Figure 1.

Schematic shows the design on Resolvin D2 loaded-nanovesicles (RvD2-HVs) that specifically bind to inflamed brain endothelium to mitigate neuroinflammation after reperfusion therapy of ischemic stroke. Generation of RvD2-HVs follows three steps: 1) nitrogen cavitation breaks cells to form nanovesicles; 2) purification of nanovesicles through a series of centrifugations; 3) loading RvD2 in nanovesicles. After intravenous (i.v.) administration, RvD2-HVs can specifically bind to inflamed brain endothelium in stroke lesions to increase delivery of RvD2 that can enhance inflammation resolution, such as inhibition of endothelial activation, cytokine release and neutrophil infiltration in ischemic sites of brain.

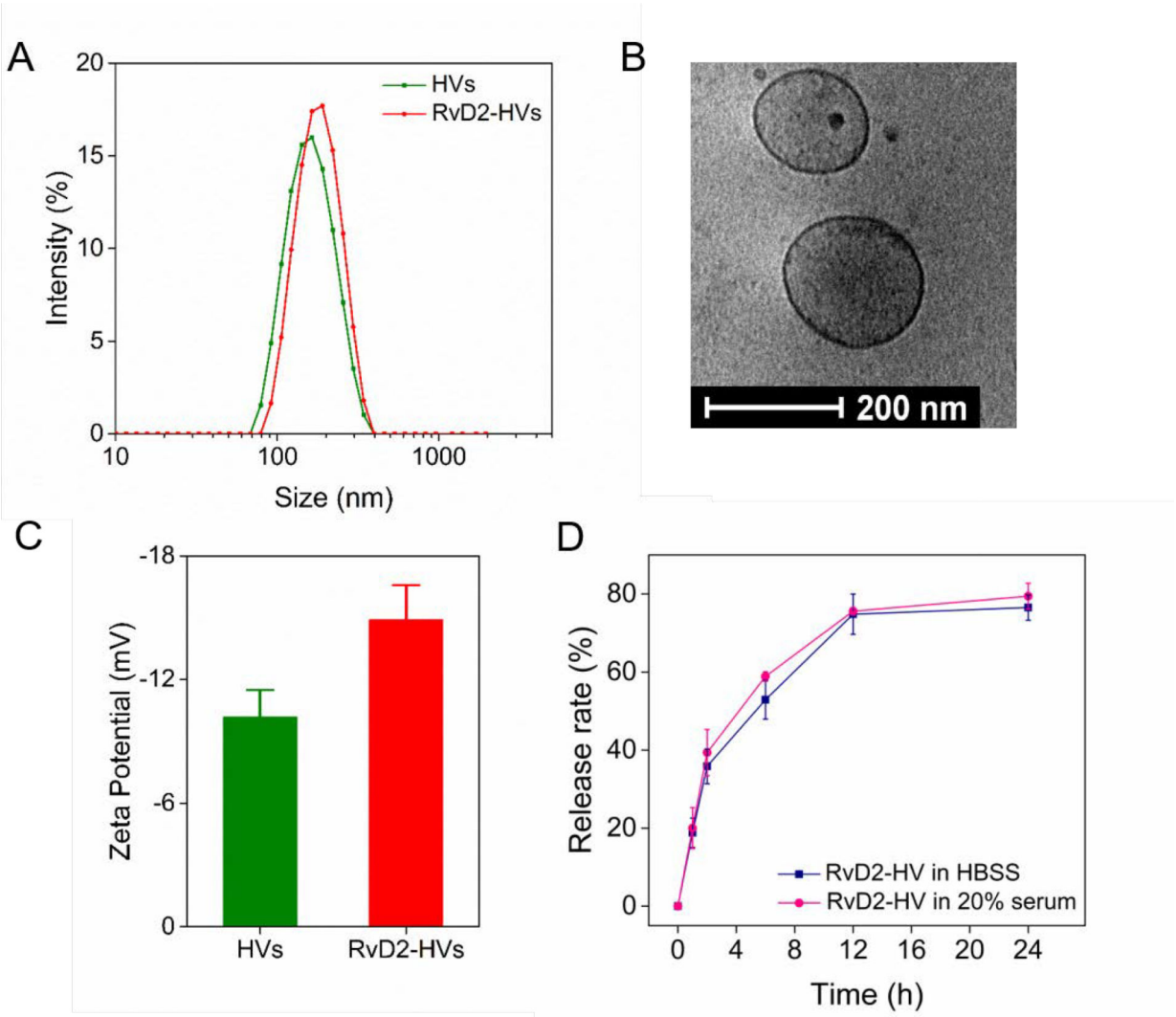

Figure 2.

Characterization of HVs and RvD2-HVs. (A) Size distribution of HVs and RvD2-HVs. (B) Cryo-EM of cell membrane-formed vesicles made from HL-60 cells. (C) Zeta potentials of nanovesicles. (D) Release profiles of RvD2 from nanovesicles. All data expressed as Mean ± SD, n=3–6.

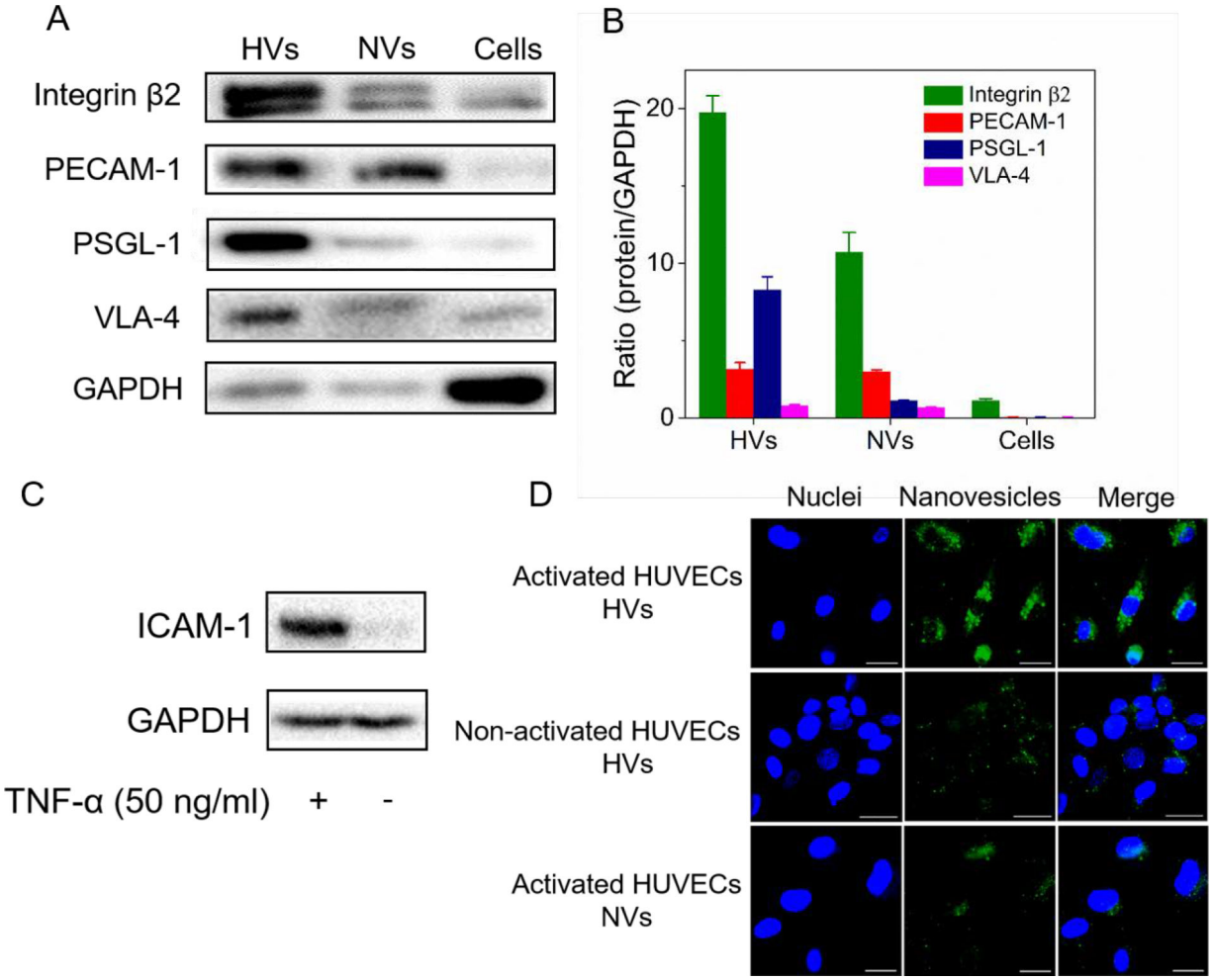

Figure 3.

In vitro studies on the binding of HVs to endothelial cells. (A) Western blot of integrin β_2, PECAM-1, PSGL-1 and VLA-4 on HL-60 nanovesicles (HVs), non-differentiated HL-60 nanovesicles (NVs) and differentiated HL-60 cells lysis (Cells). (B) Ratios of protein expression levels in HVs, NVs and cells lysis relative to GAPDH (n=3). (C) ICAM-1 expression in normal HUVECs and inflamed HUVECs induced by TNF-α. (D) Fluorescence confocal images show the binding of DiO-labeled nanovesicles (green) to inflamed HUVECs stained by DAPI (blue). (Scale bar=100 μm). HUVECs were activated by TNF-α, followed by incubation with HVs or NVs.

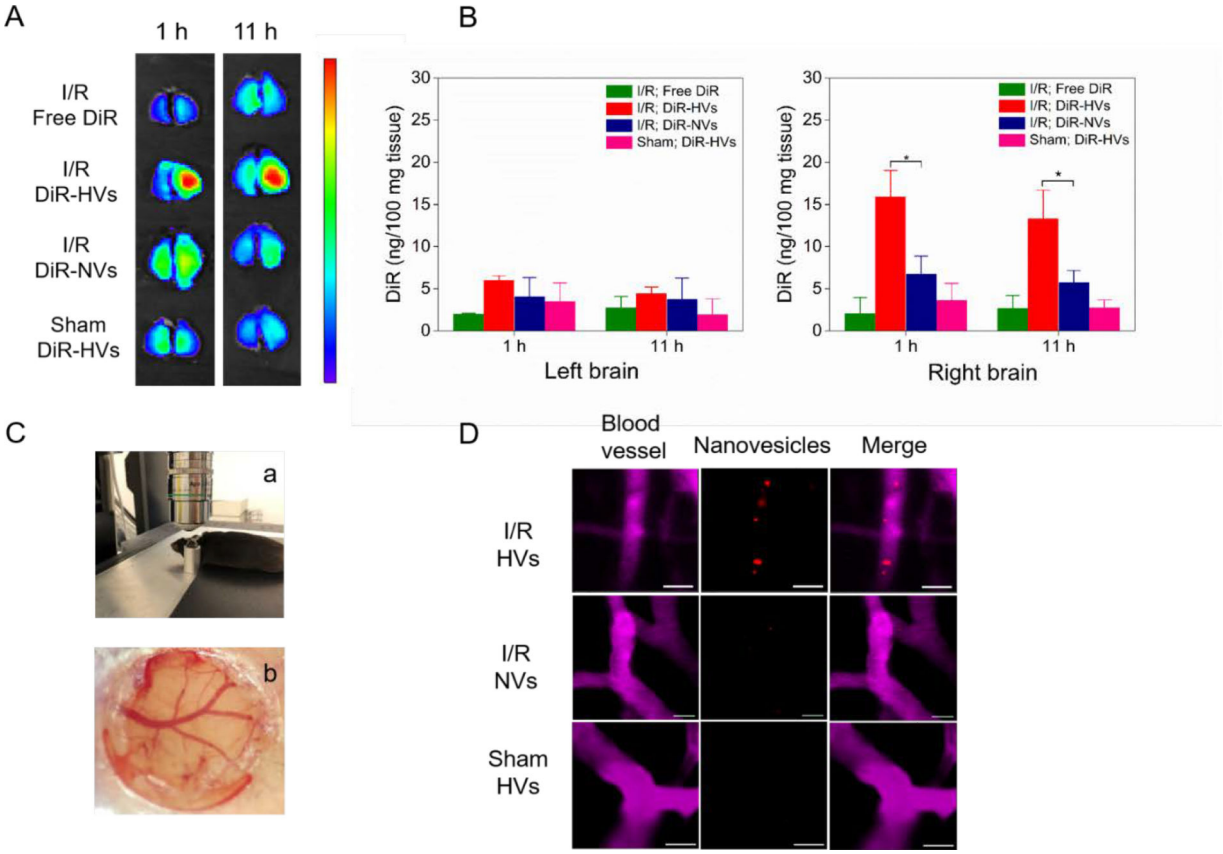

Figure 4.

Binding of nanovesicles to inflamed mouse brain is required for activation of endothelial. (A) *Ex vivo* brain images at 1 h and 11 h after injection of free DiR, DiR-vesicles (DiR-HVs) or non-differentiated DiR-vesicles (DiR-NVs) in MCAO model, and DiR-HVs in normal mice. (B) Quantification of DiR in the brain tissues in (A) after they were homogenized. All data represent as mean ± SD (n=3). (C) Cranial window is used for live mouse brain imaging. A mouse was placed on a holder during confocal microscopy (a) and a photograph shows cerebral blood vessels under cranial window (b). (D) Real-time confocal images of live mouse brain microcirculation. After MCAO surgery, several Dil labeled-HVs (red) bound to inflamed brain vasculature (top panel), while Dil-NVs were barely observed to bind to inflamed brain vasculature (middle panel). In a healthy mouse (without MCAO surgery), it was not observed that Dil-HVs bound to the brain vasculature (bottom panel). BSA-Cy5 was i.v. administered to label blood vessels (pink). Scale bar=20 μm. Two-sample Student's t test was performed (*$p < 0.05$).

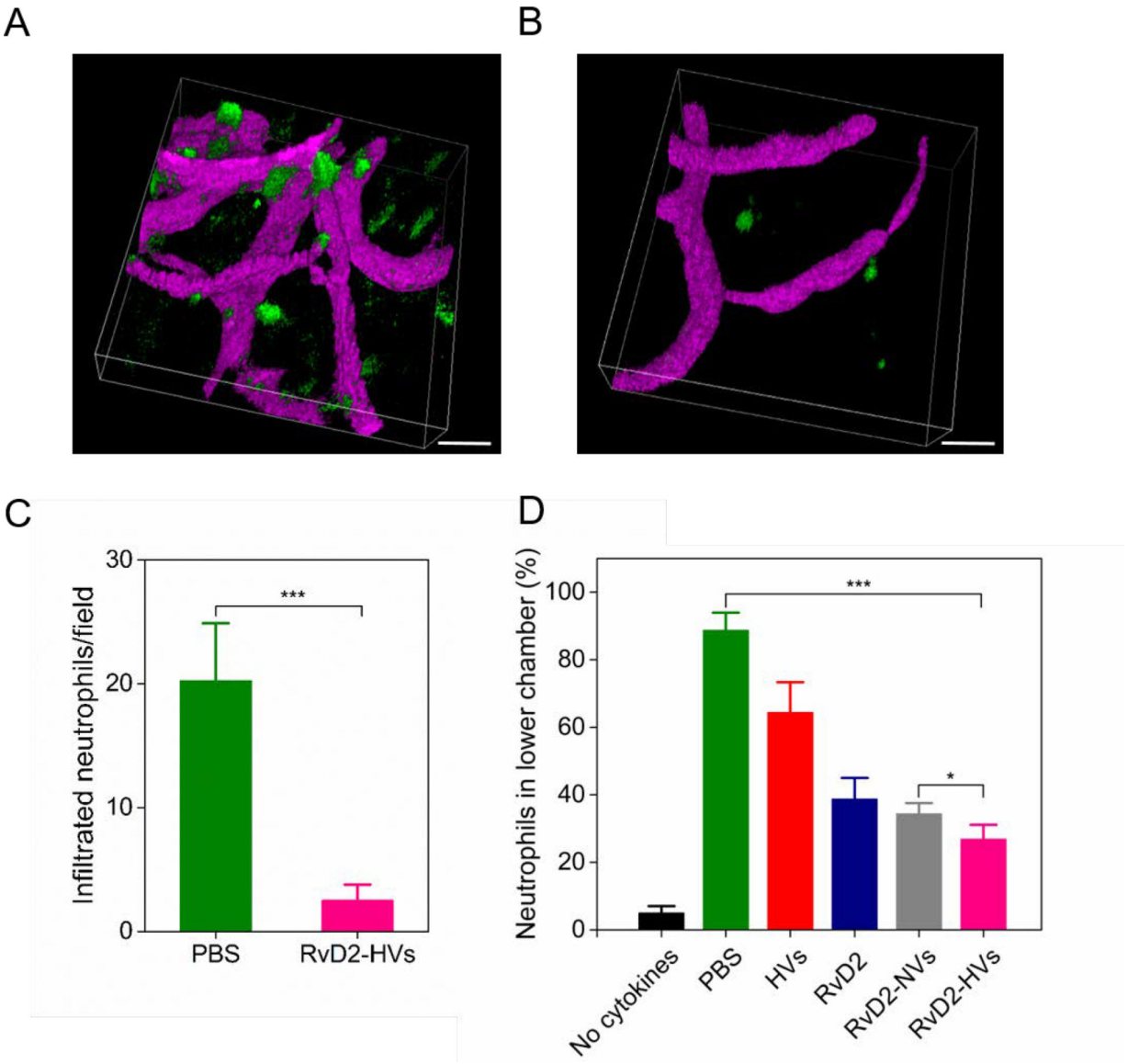

Figure 5.

RvD2-HVs reduce neutrophil infiltration *in vivo* and *in vitro*. Intravital microscopic 3D images of mouse brain show neutrophils infiltrated into inflamed brain tissues 4 h after the MCAO surgery (A) and neutrophil infiltration was significantly decreased at 2 h post-injection of RvD2-HVs (4 h after the MCAO surgery) (B). BSA-Cy5 (pink) and Alexa Fluor-488 anti-mouse Ly-6G (green) were used to label blood stream and neutrophils, respectively. Scale bar=20 μm. (C) Quantification of experiments (A) and (B). (D) Transmigration of human neutrophils studied using transwell assay after treatment with PBS, free HVs (40 μg/per assay), free RvD2 (1nM), RvD2-NVs (at 1nM RvD2) and RvD2-HVs (at 1nM RvD2). All data represent mean ± SD (n=3–6). Two-sample Student's t test was performed (*$p < 0.05$ and ***$p < 0.001$).

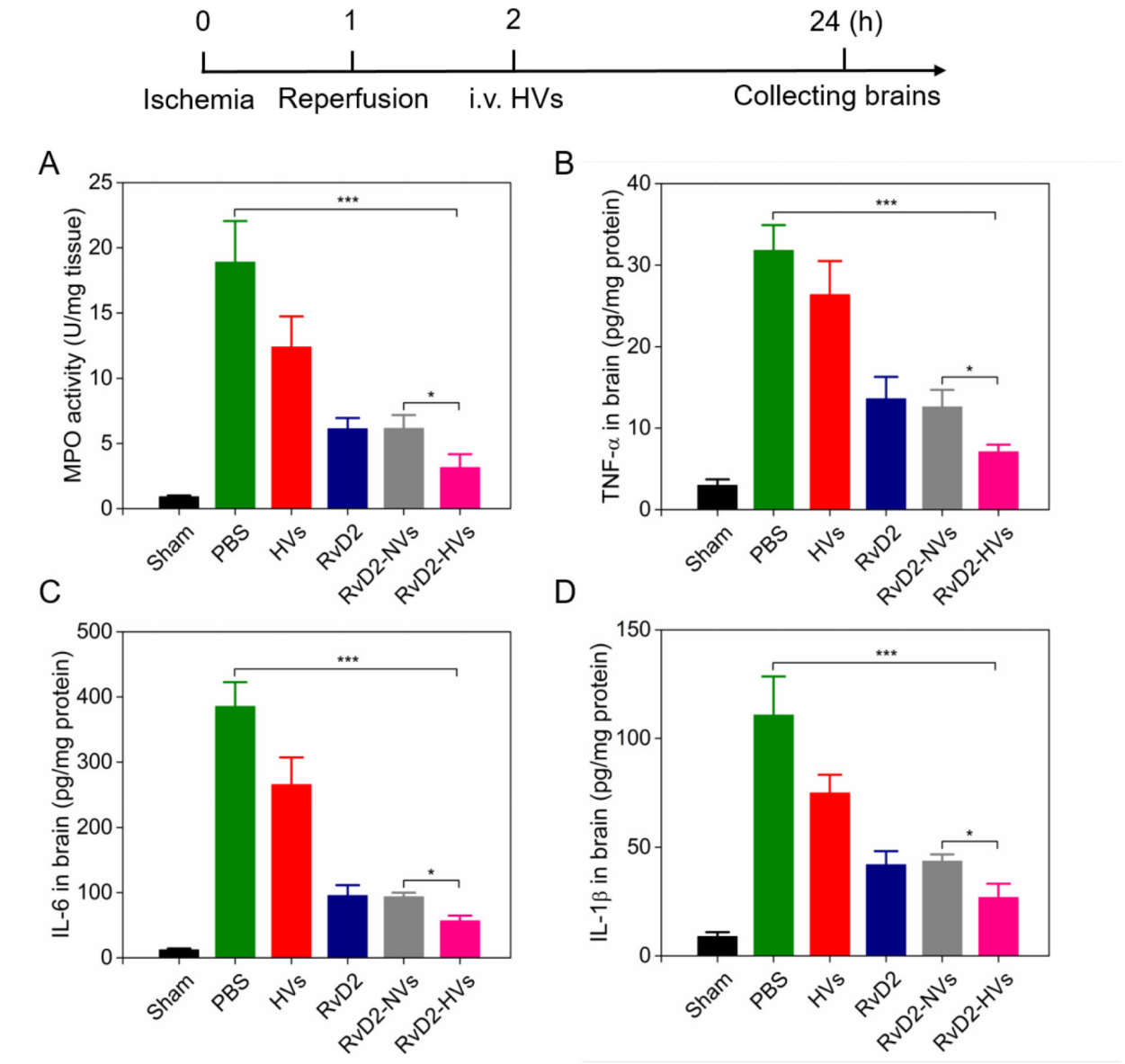

Figure 6.

RvD2-nanovesicles inhibit neutrophil infiltration and enhance inflammation resolution in brain tissues. The diagram above shows the experimental protocol. (A) MPO activity in the injured brain at 22 h post-injection of therapeutics (24 h after the MCAO surgery). Treatment with RvD2-HVs and RvD2-NVs was at RvD2 8μg/kg as same as free RvD2. Pro-inflammatory cytokines of TNF-α (B), IL-6 (C) and IL-1β (D) in injured half of brain tissues were measured. All data represent mean ± SD (n=3–6). Two-sample Student's t test was performed (*$p < 0.05$, **$p < 0.05$ and ***$p < 0.001$).

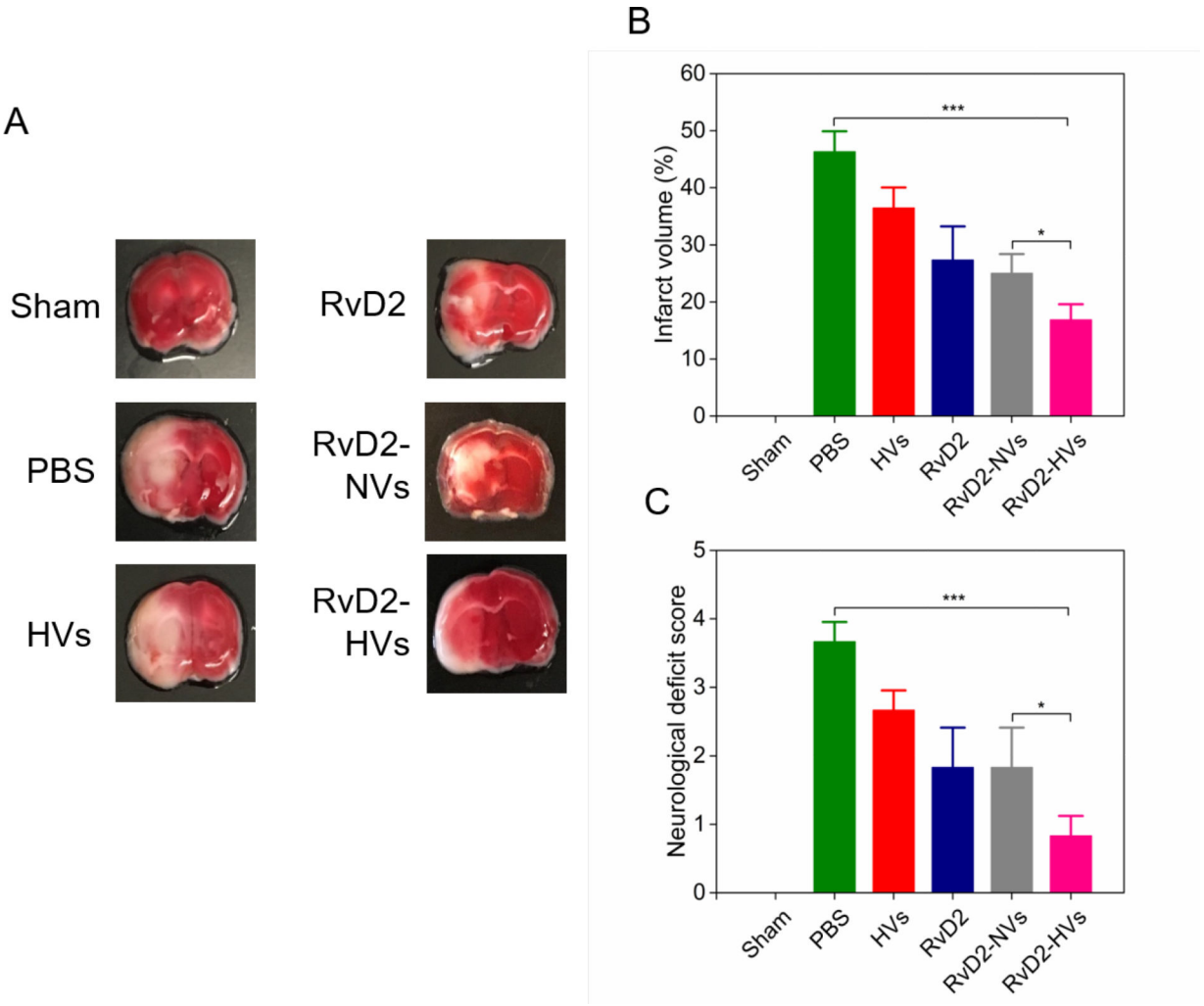

Figure 7.

RvD2-nanovesicles reduce cerebral infarct sizes and protect neurological damage from ischemic stroke at 22 h post-injection of therapeutics (24 h after the MCAO surgery). (A) Representative mouse brain sections stained with 1% of TTC in sham mice, and MCAO mice treated with PBS, HVs, RvD2, RvD2-NVs and RvD2-HVs, respectively. RvD2 was used at 8 μg/kg. Normal brain tissues appear red, but the infarct tissues appear white. (B) Infarct sizes quantified by ImageJ from Figure S8. (C) Mouse neurological deficit scores measured at 22 h post-injection of different therapeutics (24 h after the MCAO surgery). All data represent mean ± SD (n=3–6). Two-sample Student's t test was performed (*$p < 0.05$ and ***$p < 0.001$).